NRL Memorandum Report 4967

Multidimensional Numerical Methods for the Simulation of Shock-Generated Turbulence

J. M. PICONE AND J. P. BORIS

Laboratory for Computational Physics

December 30, 1982

NAVAL RESEARCH LABORATORY
Washington, D.C.

SECURITY CLASSIFICATION OF THIS PAGE (When Data Entered)

REPORT DOCUMENTATION PAGE		READ INSTRUCTIONS BEFORE COMPLETING FORM
1. REPORT NUMBER NRL Memorandum Report 4967	2. GOVT ACCESSION NO. AD-A123235	3. RECIPIENT'S CATALOG NUMBER
4. TITLE (and Subtitle) MULTIDIMENSIONAL NUMERICAL METHODS FOR THE SIMULATION OF SHOCK-GENERATED TURBULENCE		5. TYPE OF REPORT & PERIOD COVERED Interim report on a continuing NRL problem 6. PERFORMING ORG. REPORT NUMBER
7. AUTHOR(s) J. M. Picone and J. P. Boris		8. CONTRACT OR GRANT NUMBER(s)
9. PERFORMING ORGANIZATION NAME AND ADDRESS Naval Research Laboratory Washington, D. C. 20375		10. PROGRAM ELEMENT, PROJECT, TASK AREA & WORK UNIT NUMBERS 61153N, 44-1529-0-2, ~~RR41-2;~~ 61101E, 44-0580-0-2
11. CONTROLLING OFFICE NAME AND ADDRESS Office of Naval Research, Arlington, VA 22217 and Defense Advanced Research Projects Agency, Arlington, VA 22209		12. REPORT DATE December 30, 1982 13. NUMBER OF PAGES 17
14. MONITORING AGENCY NAME & ADDRESS(if different from Controlling Office)		15. SECURITY CLASS. (of this report) Unclassified 15a. DECLASSIFICATION/DOWNGRADING SCHEDULE

16. DISTRIBUTION STATEMENT (of this Report)

Approved for public release; distribution unlimited.

17. DISTRIBUTION STATEMENT (of the abstract entered in Block 20, if different from Report)

18. SUPPLEMENTARY NOTES

This research was supported by the Office of Naval Research and by the Defense Advanced Research Projects Agency (DoD) ARPA Order No. 4395, Amendment 1.

19. KEY WORDS (Continue on reverse side if necessary and identify by block number)

Numerical methods
Hydrodynamics
Turbulence
Laser Channels
Electric discharge channels

20. ABSTRACT (Continue on reverse side if necessary and identify by block number)

We discuss shock-generated turbulence as related to the dynamics of hot gaseous channels produced by laser pulses and electric discharges in gaseous atmospheres. Accurate models of channel development must account for compressible flows, which are associated with shocks that are present at early times, as well as the incompressible residual motion which is responsible for channel cooling. We present an efficient numerical technique which uses the flux-corrected transport algorithm and permits automatic adjustment of the time step to account for both types of behavior. Comparisons of two-dimensional calculations to theory and to experimental data
(Continued)

DD FORM 1 JAN 73 1473 EDITION OF 1 NOV 65 IS OBSOLETE
S/N 0102-014-6601

SECURITY CLASSIFICATION OF THIS PAGE (When Data Entered)

20. ABSTRACT (Continued)

on laser channels show good agreement. Our numerical results reveal a mechanism by which the distribution of turbulent scale lengths is generated during energy deposition.

CONTENTS

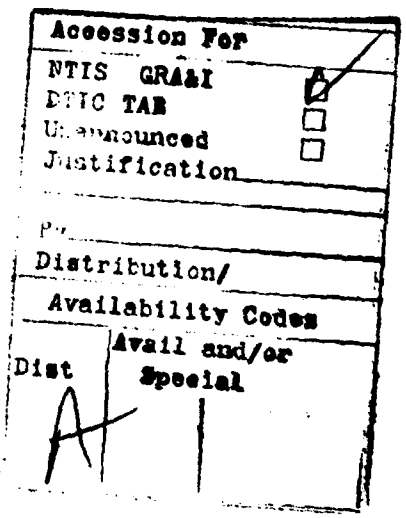

MULTIDIMENSIONAL NUMERICAL METHODS FOR THE SIMULATION OF SHOCK-GENERATED TURBULENCE

I. THE PHYSICS OF HOT GASEOUS CHANNELS

Recent experimental studies of electric discharges in air and laser pulses in air and pure nitrogen [1-2] have revealed the detailed dynamics of the hot gaseous channels which remain. The production and cooling of such hot, gaseous channels is of interest not only in laser and discharge experiments, but also in research on the physics of lightning and electron beams. During and immediately after energy deposition, the resulting hot gas quickly expands to achieve pressure equilibrium with the surrounding atmosphere, producing a shock wave which propagates away in a short time. The channel then cools on time scales which are orders of magnitude faster than those characterizing classical (nonturbulent) thermal conduction. As a channel cools, the radius increases according to the equation

$$R^2(t) = R^2(\tau) + 4\alpha\,(t-\tau), \qquad (1)$$

where R is the radius of the channel, t is time measured from the beginning of a discharge or pulse, $t=\tau$ is the time at which pressure equilibrium is reached, and α is the thermal diffusivity. For electric discharges which deposit $\approx$ 300-600 J/m, measurements at early times give $\alpha \approx 500$ cm^2/s [1]. The experimental CO_2 laser pulses in nitrogen deposit $\approx$ 9 J/m, giving $\alpha \approx 250$ cm^2/s [2]. For nonturbulent thermal conduction, we have $\alpha = 1.0$ cm^2/s for air at 800K and 1 atm [3].

As a channel cools, turbulent structure appears first at the boundary and then in the interior. This has led us naturally to search for mechanisms in which long-lived rotational motion is produced. The only successful analysis to date [1,4] relies on the (rigorous) equation for the time development of vorticity, i.e.,

Manuscript approved September 22, 1982.

$$\frac{d\underset{\sim}{\xi}}{dt} + \underset{\sim}{\xi}\underset{\sim}{\nabla} \cdot \underset{\sim}{v} = \underset{\sim}{\xi} \cdot \underset{\sim}{\nabla v} + (\underset{\sim}{\nabla}\rho \times \underset{\sim}{\nabla}P)/\rho^2 \quad , \tag{2}$$

where $\underset{\sim}{\xi} = \underset{\sim}{\nabla} \times \underset{\sim}{v}$ is the vorticity, $\underset{\sim}{v}$ is the fluid velocity, ρ is the density, and P is the pressure. According to eq. (2), any misalignment between the pressure and density gradients during expansion of the gas to pressure equilibrium will generate vorticity. This will occur when asymmetries exist in the structure of a pulse and when consecutive pulses are noncollinear. After pressure equilibrium is reached, we may represent the flow field in terms of one or more pairs of vortex filaments of strength $\pm\kappa$, where

$$\kappa = U_m (R_1 - R_0) \ln (\rho_\infty/\rho_0) f. \tag{3}$$

In eq. (3), U_m is a characteristic expansion velocity; R_0 is the initial channel radius; R_1 is the radius of the channel just after expansion to pressure equilibrium; ρ_∞ is the ambient density; ρ_0 is the density at the center of the channel; and $f(\lesssim 1)$ is a form factor. The number of vortex filament pairs depends on the situation.

II. NUMERICAL MODEL

An accurate numerical model of channel dynamics is necessary for the solution of problems which are too difficult to treat analytically, as well as for the verification and calibration of our theoretical results [1,4]. We favor the use of a finite difference scheme to integrate the equations for conservation of mass, momentum, and energy. A major complication is the fact that the flows which generate vorticity are supersonic and require short time steps, as dictated by the Courant condition, while the (incompressible) residual flows, which are responsible for channel cooling, could be computed with much longer time steps ($\lesssim$ 100 x). The model which we describe below includes a simple, effective method of numerically separating the rotational flows from the (radial) shock flows at times when the latter are no longer important near

the channel. This permits the adjustment of the time step to account for the slower flows, saving considerable computer time.

Our calculations are multidimensional, using time-step splitting in conjunction with the latest version of flux-corrected transport (FCT) [5]. The grid is Cartesian and is uniform and finely spaced in the region near the channel. Outside of this fine grid, the cells increase geometrically so that the boundaries are far from the channel. This permits the shock to decouple completely from the channel before interacting with the boundary. After the shock has moved well away (> 10 channel radii) from the channel, the pressure field near and within the channel is approximately ambient. At this point, we calculate and subtract the average radial velocity field from the total velocity field, leaving only the rotational flows of interest. To compute this average radial velocity field, we use the following self-consistent method, based on digital multichannel analysis:

(1) Relative to the center of the channel, define a set of contiguous radial intervals which encompass the entire differencing grid, as shown in fig. 1.

(2) For each interval, determine the grid points whose radial displacements from the channel center fall within the interval. Average the radial velocity components of these grid points.

(3) From this average radial velocity field, denoted $\langle v_r \rangle$, determine the average radial potential function by integrating the Poisson equation,

$$\nabla^2 \phi = \nabla_r \langle v_r \rangle .$$

(4) Interpolate the field $\langle v_r \rangle$ onto the grid by straightforward differencing of the equation $\nabla_r \phi = \langle v_r \rangle$ to maintain consistency with the differencing solution for the total velocity field.

(5) Subtract the field $\langle v_r \rangle$ from the total velocity field at each grid point.

(6) Set the pressure field to the ambient value and set the velocities near and at the shock wave to zero to eliminate all high speed flows and to prevent shock interaction with the boundary.

Immediately after the above sequence, we must increase the size of the time step, since the flows of interest are much slower than the sound speed. Our use of FCT, however, requires that the Courant condition be satisfied. We accomplish this by scaling the pressure down by a factor β, so that $P \rightarrow P/\beta$ and $c_s \rightarrow c_s/\beta^{1/2}$, where the local speed of sound is $c_s = (\gamma P/\rho)^{1/2}$ and γ is the ratio of principal specific heats. The time step will scale roughly as $\Delta t \rightarrow \beta^{1/2}\,\Delta t$. O'Rourke and Bracco [6] have employed a similar scaling technique to reduce the computational time required to model unsteady laminar flames using multidimensional, fully compressible computer codes. In their method, the speed of sound remains the same while the velocity and other related parameters are scaled to larger values. The transformation of O'Rourke and Bracco thus artifically increases the speed of the flow relative to the speed of sound while permitting a time step which is approximately the same as that which would have been dictated by the Courant condition prior to scaling. Both the scaling method used by us and that of O'Rourke and Bracco increase the Mach number of the flow to reduce the effect of the Courant condition on total computing time.

An appropriate value of β will insure that the errors introduced by our technique are small. Setting the pressure field to the ambient value in step (6) above will initially eliminate the minute pressure gradients which maintain the rotational motion of the fluid. This will permit the velocity field in the vicinity of a vortex filament to expand momentarily. The expansion, however, reduces the local density and pressure approximately adiabatically until the pressure gradients again counteract the centrifugal force experienced by a given fluid element. In the Appendix we show that the effect on the vorticity ξ is of order v^2/c'^2_s, where $c'_s \equiv c_s/\beta^{1/2}$ is the speed of sound after scaling. In practice we choose β so that $v/c' \lesssim 1/5$ to insure that such errors are small. Another important concern is the effect of scaling on the incompressibility of the residual flow field. Since errors

related to compressible effects for a subsonic flow field are also of order v^2/c_s^2 [7], our constraint on β again insures that such errors are less than a few percent. Should β be too large, we would expect some energy to be diverted to the formation of compressional waves, resulting in a reduction in intensity of the rotational motion. Our calculations have verified that the flow pattern remains rotationally stable and accurate for several simulated milliseconds after our procedure is performed. The residual vorticity has proven to be correct to first order, as expected, and no compressional waves have arisen at late times, again supporting our analysis.

III. NUMERICAL SIMULATIONS

All numerical simulations to date have used a Cartesian grid of 100 x 100 cells. The central region, where energy is deposited, consists of 50 x 50 square cells chosen so that an individual pulse would be contained in an area no smaller than 8 x 8 cells. Outside the uniform central region, each cell dimension increases geometrically by a factor $(1+\delta)$ from cell to cell, where $\delta<0.3$, so that the grid boundary is far from the channel. All pulses initially have a Bennett pressure profile

$$P(\underset{\sim}{r}) = P_\infty + (P_0-P_\infty)/(1+\frac{|\underset{\sim}{r}-\underset{\sim}{r}_0|^2}{a^2})^2 \quad , \qquad (4)$$

where P_0 is the pressure at the center of the pulse, P_∞ is the ambient pressure, $\underset{\sim}{r}_0$ is the position of the center of the pulse, and a is a constant (the "Bennett radius"). The model deposits all energy instantaneously in the form of an increase in internal energy. We use a real air equation of state routine based on the data of Gilmore [8-9].

As our first example, we choose the simple case of noncollinear pulses produced at different times. The first pulse deposits energy at time t=0.0 in the center of the grid, and the second pulse occurs 1 ms later and is displaced to the (reader's) right of the first by a distance equal to the Bennett radius (a=0.5cm). The initial peak overpressures (P_0-P_∞) of the pulses are 4.7 atm and 2.4 atm, respectively.

Figure 2 shows density contours and velocity vectors in the finely gridded region at t=1.26 ms and density contours at t=2ms. The contours range from 3.0×10^{-4} g/cm^3 at the center of the grid to 1.1×10^{-3}g/cm^3 at the edge. From Fig. 2a we see that the noncollinearity of the pulses produces a noncircular channel cross section. The velocity vector plot clearly demonstrates the presence of a vortex filament pair whose flow pattern pulls fluid from the position of the first pulse toward that of the second. Figure 2c shows that the gas at the center of the system has cooled under the influence of the residual flows. These features are in complete agreement with theoretical predictions [4] based on Eq. (2) and (3).

A more important and difficult case is that of a laser pulse with an approximately circular envelope. Although turbulent cooling might appear to be less important in this situation, experimental data for a laser pulse in nitrogen at 1.2 atm give $\alpha \approx 250\text{cm}^2/\text{s}$. Laboratory burn patterns have also revealed that nonuniformities ("hot spots") exist in the interior of the laser pulse. We have used this fact in a test calculation in which the actual laser pulse is assumed to consist of seven smaller, identical, simultaneous pulses, as in the pressure contour diagram of Fig. 3a. Again we show only the uniform central region of the grid, which is 1.2 cm x 1.2 cm. The energy deposited per unit length is $\approx$ 9 J/m, in agreement with experiment [2]. We use the real air equation of state routine (rather than one for nitrogen) and 1.0 atm ambient pressure. The pressure contours range from 1.1×10^6 dyne/cm^2 to 3.0×10^6 dyne/cm^2 while the density contours in the remaining diagrams range from 5.7×10^{-4} g/cm^3 to 1.1×10^{-3} g/cm^3. The rather mild hot spots in Fig. 3a would be marginally detectable by a burn pattern. From Fig. 3a, we see that the shock wave produced by each hot spot will sweep through the density minima occurring at the positions of the other hot spots, producing vorticity according to Eq. (2). By t=56μs, the channel has achieved pressure equilibrium and a temperature of $\lesssim$ 650K. The envelope is nearly circular, even though nonuniformities persist in the interior of the channel. Because the grid is rather coarse and does not have sixfold symmetry and

because we use time-step splitting, the channel properties do not retain the exact sixfold symmetry of Fig. 3a. The use of a finer grid, and perhaps multidimensional FCT [10], would improve the situation, although multidimensional FCT is slower (≈2x) and requires more storage space, as compared to the algorithm used here. At later times, the boundaries distort under the influence of local vortex filament pairs, and the channel dimensions increase. When viewed from a direction perpendicular to the channel axis, the channel should appear to expand, and the boundary distortions should appear as striations parallel to the channel axis. These features are in fact present in Schlieren photographs. Our calculation yields $\alpha \sim 1$[illegible] cm^2/s, which is within a factor of 2.5 of the experimental value [2].

IV. CONCLUDING REMARKS

This method for calculating the generation of turbulence by shocks and the subsequent cooling of hot gaseous channels has proven to be accurate and efficient. We have reproduced theoretical predictions for consecutive, noncollinear pulses and have verified features observed experimentally for laser channels in air. Viewing the diagrams in Fig. 3, we find that the scale lengths of nonuniformities within the laser pulse will determine the scale lengths appearing in the turbulent structure. The resolution provided by the numerical grid, however, places a lower limit on the distribution and could affect the interactions between turbulent structures of various sizes.

ACKNOWLEDGEMENTS

We gratefully acknowledge the support of the Defense Advanced Research Projects Agency (DARPA Order No. 4395, Amendment 1) and the Office of Naval Research. Conversations with M. Lampe, R. Greig, M. Raleigh, R. Fernsler, M. Fry, and R. Quirguis have proven most helpful.

REFERENCES

1. J.M. Picone, J.P. Boris, J.R. Greig, M. Raleigh, and R.F. Fernsler, J. Atmos. Sci., 38 (9), 2056-62 (1981).
2. J.R. Greig, R.E. Pechacek, M. Raleigh, and K.A. Gerber, NRL Memo Rep. 4826 (1982)
3. G.K. Batchelor, An Introduction to Fluid Dynamics (Cambridge University Press, New York, 1967), Appendix 1, p. 594.
4. J.M. Picone and J.P. Boris, "Vorticity Generation by Asymmetric Energy Deposition in a Gaseous Medium," submitted to Phys. Fluids.
5. J.P. Boris and D.L. Book, Methods in Computational Physics, Vol. 16 (Academic Press, New York, 1976), pp. 85-129.
6. P.J. O'Rourke and F. V. Bracco, J. Comp. Phys., 33 (2), 185-203 (1979).
7. A.H. Shapiro, The Dynamics and Thermodynamics of Compressible Fluid Flow, Vol.1 (Wiley, New York, 1953), Chapter 10.
8. F.R. Gilmore, RAND Corp. Rep. RM-1543 (1955).
9. F.R. Gilmore, Lockheed Missile and Space Co. Rep. DASA 1917-1 (1967).
10. S.T. Zalesak, J. Comput. Phys., 31 (3), 335-362 (1979).

MULTICHANNEL AVERAGING

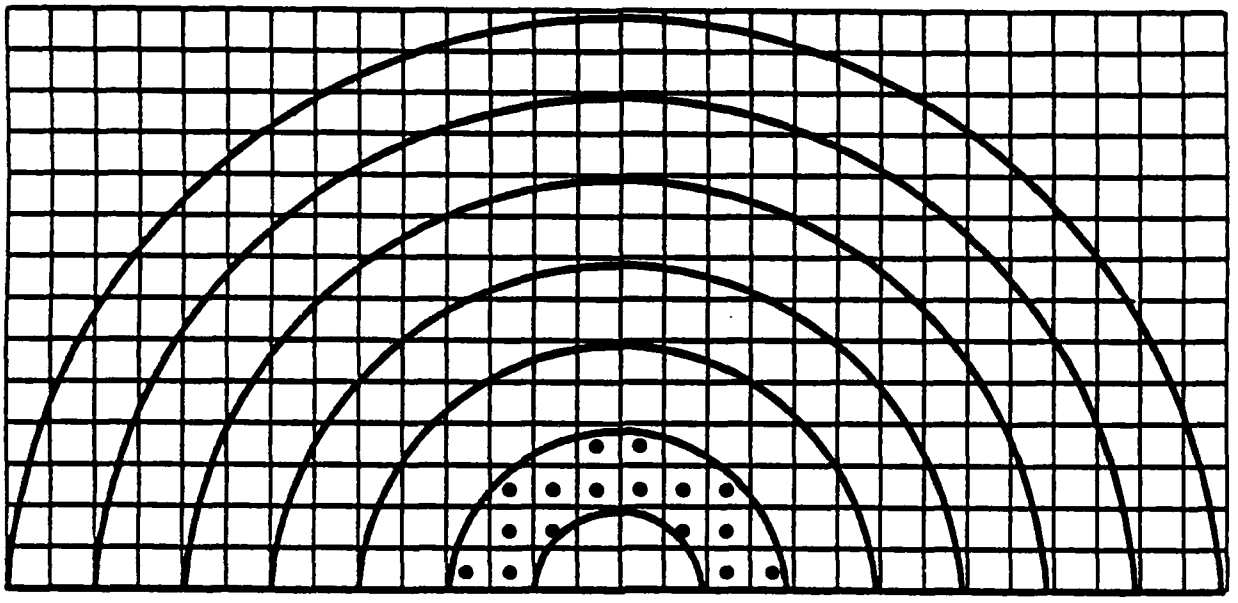

$$v_c^{av} = \sum_{i=1}^{N_c} v_i / N_c$$

Fig. 1 — Schematic diagram showing a portion of the upper half of the grid in order to demonstrate the method of obtaining the average radial velocity. We divide the grid into radial channels, each two cells wide in this example, and average the radial velocities at all cell centers falling within a particular radial channel. We label each channel by an integer, denoted "c" in the equation. The black dots indicate the cells involved when $c = 2$. For the problems discussed in this paper, we center the radial channels on the latest pulse.

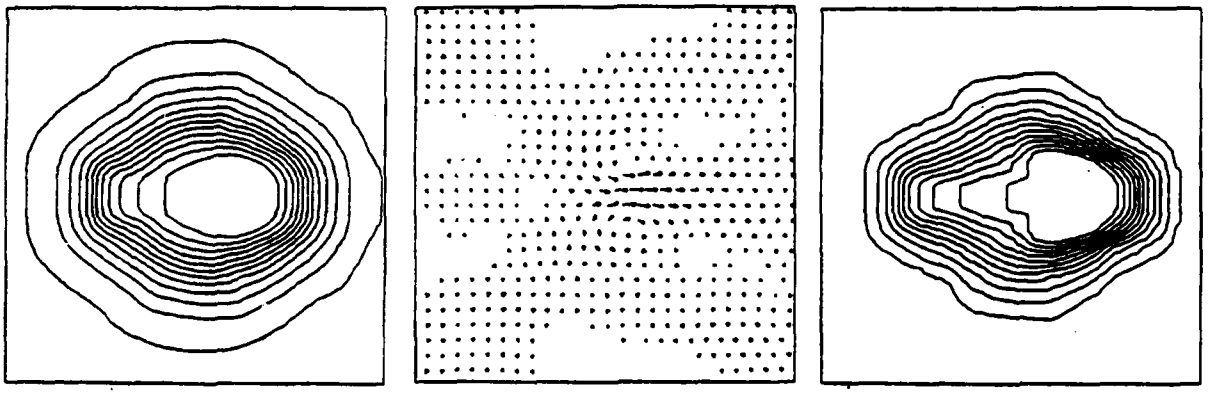

(a) 1.26 ms (b) 1.26 ms (c) 2.0 ms

Fig. 2 — Density contour diagrams and velocity vector plot for the case of two noncollinear, nonsimultaneous pulses. The first pulse occurs at $t = 0.0$ μs and the second at $t = 1.0$ ms. The appropriate time appears below each diagram.

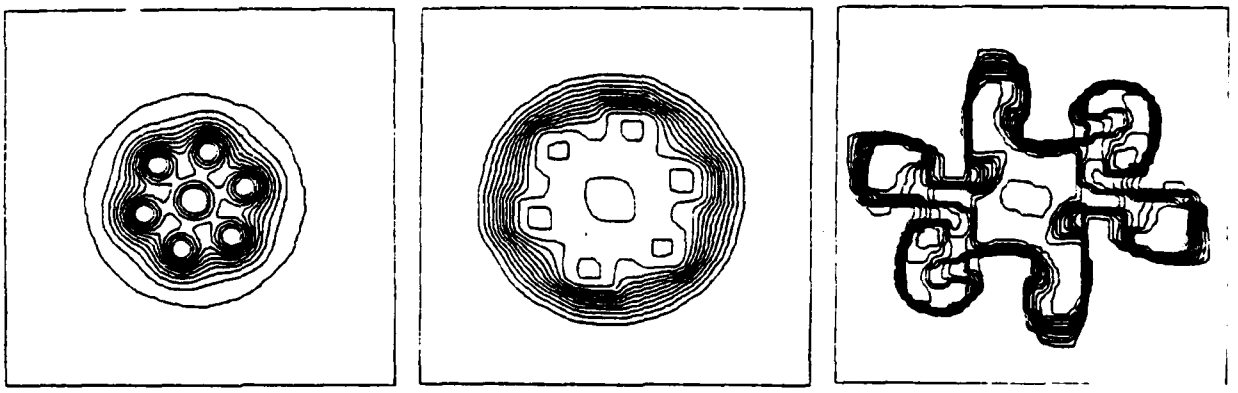

(a) 0.0 μs (b) 56 μs (c) 1.24 ms

Fig. 3 — (a) Pressure contours and (b), (c) density contours for the case of a laser pulse with a circular envelope and a nonuniform interior. Energy deposition occurs at $t = 0.0$ μs. The appropriate time appears below each diagram.

APPENDIX

Here we discuss in detail the errors incurred by our procedure for eliminating the shock wave in our simulation and by our subsequent scaling of the pressure to reduce the speed of sound, thereby increasing the size of the time step permitted by the Courant condition. After the shock wave has moved well away from the channel, we may represent the residual flow field near the channel as a superposition of vortex filaments. For our estimate, we consider an isolated, cylindrically symmetric vortex filament of finite radius A. By definition the vorticity $\underset{\sim}{\xi}=0$ for $r > A$, where r is the radial cylindrical coordinate and the z-axis coincides with the axis of the filament. The vortex filament strength (or the circulation) is thus

$$\kappa(R) \equiv \int_{S(R)} \underset{\sim}{\xi} \cdot d\underset{\sim}{a} \tag{1}$$

in which S(R) is the cross-sectional area of a cylinder centered on the z-axis and having a radius R. From eq. (1) and the definition above, $\kappa(R) = \kappa(A)$ for $R > A$. The velocity field is azimuthally symmetric,

$$\underset{\sim}{v}(R) = v(R)\underset{\sim}{e}_\phi = \frac{\kappa(R)}{2\pi R}\,\underset{\sim}{e}_\phi \,. \tag{2}$$

Before our techniques are implemented, the velocity field of the vortex is directly related to the pressure through the radial acceleration a_r experienced by a fluid element at radius R,

$$\frac{v^2}{R} = -a_r = \frac{1}{\rho}\nabla_r P, \tag{3}$$

where we have suppressed the functional dependence of the variables on R. For the cases of interest, we have $\rho v^2 \ll P$, so that the speed of a fluid element is small compared to the sound speed c_s. For simplicity, we could assume that $\underset{\sim}{\xi}$ is constant and directed along the z-axis. Then Eq. (1) becomes

$$\kappa(R) = \pi R^2 \xi \tag{4}$$

and Eq. (2) gives us

$$v = \begin{cases} \frac{\xi R}{2}, & R < A \\ \\ \frac{\xi A^2}{2R}, & R > A \end{cases} . \tag{5}$$

Now we employ our procedure for eliminating the shock wave and increasing the size of the time step. To do so we set the entire pressure field to the ambient value and scale the pressure by a factor β, so that

$$P \to P_\infty \to P'_\infty = P_\infty/\beta. \tag{6}$$

After this occurs, the minute pressure gradient in eq. (3) no longer exists, and the fluid will consequently expand. Expansion will continue until pressure gradients satisfying eq. (3) again exist. The fluid variables will have undergone the following transformation:

$$\begin{aligned} P' \equiv P'_\infty &\to P'^* < P'_\infty \\ \rho &\to \rho^* < \rho \\ v &\to v^* < v \\ \xi &\to \xi^* < \xi \end{aligned} \tag{7}$$

in the region where the vorticity is nonnegligible. In eq. (7), the asterisk (*) signifies the value after expansion, and all variables after expansion depend on R. The density and pressure will quickly approach ambient values outside of the radius $A^*(>A)$ at which the vorticity ξ^*

falls to a negligible value. For our rather crude estimate, we average the variables over the region $R \in (0, A^*)$ to obtain values representative of the interior of the expanded vortex filament. In the paragraph below, any variable marked by an asterisk will denote this average value.

The proper choice of the scaling variable β will insure that $P'_\infty >> \rho^* v^{*2}$, and the expansion will be brief and approximately adiabatic. We then have

$$\begin{aligned} P'^* &\sim P'_\infty - \delta P' \\ \rho^* &\sim \rho - \delta\rho \\ v^* &\sim v - \delta v \\ \xi^* &\sim \xi - \delta\xi \ , \end{aligned} \tag{8}$$

where the quantities $\delta P'$, $\delta\rho$, δv, $\delta\xi$ are all small quantities. To compute the effects of the expansion, we use the adiabatic gas law:

$$\frac{P'^*}{P'_\infty} = \left(\frac{\rho^*}{\rho}\right)^{\gamma'} \tag{9}$$

where γ' depends on P'_∞ and ρ and is approximately constant during the expansion. Using eq. (8) in eq. (9), we obtain

$$\frac{P'_\infty - \delta P'}{P'_\infty} \sim \left(\frac{\rho - \delta\rho}{\rho}\right)^{\gamma'} \sim 1 - \frac{\gamma' \delta\rho}{\rho} \ . \tag{10}$$

Using the expression

$$\nabla_r P \sim \frac{P'_\infty - P'^*}{A^*} \sim \frac{\delta P'}{A^*} \tag{11}$$

in eq. (3) with $R = A^*$, where the centrifugal force is a maximum (see eq. (5)), we obtain

$$\rho^* v^{*2} \sim \delta P' \tag{12}$$

Notice that the variables before scaling also satisfy a similar relation,

$$\rho v^2 \sim \delta P \tag{13}$$

where

$$\delta P \sim \delta P' . \tag{14}$$

Thus we have

$$\rho v^2 \sim \delta P' \sim \rho^* v^{*2} . \tag{15}$$

Using eq. (15) to substitute for $\delta P'$ in eq. (10), we obtain

$$1 - \frac{\gamma' \delta\rho}{\rho} \sim 1 - \frac{\rho v^2}{P'_\infty} , \tag{16}$$

or

$$\frac{\delta\rho}{\rho} \sim \frac{\rho v^2}{\gamma' P'_\infty} \approx \frac{v^2}{c'^2_s} . \tag{17}$$

where c_s' is the average speed of sound after scaling, but prior to expansion. Because vorticity and mass are conserved for a given fluid element, we have from eq. (8)

$$\frac{\xi^*}{\xi} = \frac{\rho^*}{\rho} \approx 1 - \frac{\delta\rho}{\rho} \sim 1 - \frac{v^2}{c'^2_s} . \tag{18}$$

Eq. (18) demonstrates that the average change in the vorticity will be of order $v^2/c_s'^2$. A value of $v/c_s' \sim 0.2$ means that we will pay essentially no execution cost premium using explicit FCT vis-a-vis an implicit method. The use of an explicit FCT method ensures that errors of $\lesssim 4\%$ are the worst to be expected.